Asian Journal of Chemistry; Vol. 37, No. 2 (2025), 447-454

ASIAN JOURNAL OF CHEMISTRY

https://doi.org/10.14233/ajchem.2025.33308

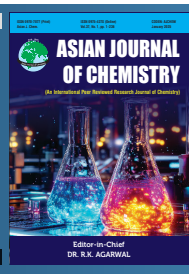

Synthesis of Cu_2O Nanoparticles Supported on Mesoporous Carbon: Highly Efficient Catalyst for Synthesis of Triazoles

RAMESH ANUMANDLA[1], JAGADISH TOTA[2], PRAGATHI JOGI[3], S. PRAKASH[1], VARUKOLU MAHIPAL[4], G. VINOD[5] and V. SHASHIKALA[1,6,*]

[1]Department of Chemistry, University College for Women, Osmania University, Hyderabad-50001, India
[2]Department of H&S (Chemistry), CVR College of Engineering, Hyderabad-501510, India
[3]G. Narayanamma Institute of Technology and Sciences, Hyderabad-500104, India
[4]Department of Chemistry, St. Peters Engineering College, Hyderabad-500100, India
[5]Department of Humanities & Science (Physics), Teegala Krishna Reddy Engineering College, Medbowli, Hyderabad-500097, India
[6]Department of Chemistry, Veeranari Chakali Ilamma Women's University, Hyderabad-500001, India

*Corresponding author: E-mail: shashikala_chem@osmania.ac.in

Received: 13 December 2024; *Accepted*: 18 January 2025; *Published online*: 31 January 2025; AJC-21897

Triazoles are class of heterocyclic compounds with significant pharmaceutical and industrial applications. An effective catalyst for the synthesis of triazoles using the Click reaction is developed. Highly stable cuprous oxide nanoparticles were dispersed on active carbon prepared from palmyra palm fruit shells. The Cu_2O nanoparticles, characterized by their small particle size and high surface area, were successfully synthesized and supported on activated carbon to enhance the catalytic efficiency. Thus, the prepared catalyst exhibited excellent catalytic activity, high selectivity and good reusability in the cycloaddition reaction of azides and alkynes, leading to the efficient synthesis of various triazole derivatives. The Cu_2O-AC nanocomposites demonstrated the superior catalytic performance compared to pure Cu_2O and activated carbon. All Cu_2O supported and unsupported active catalysts were characterized using XRD, FT-IR, SEM and EDX techniques to know the morphology, phase and functional group analysis. The reaction mechanism was investigated using density functional theory (DFT) analyses.

Keywords: Triazole, Click reaction, Cuprous oxide, Activate carbon, Dispersion.

INTRODUCTION

Nanoparticle catalysts exhibit superior activities in comparison to bulk surfaces. This enhancement is attributed to their high surface-to-volume ratio and the presence of newly exposed sites, which contribute to their elevated intrinsic activity. Moreover, nanoparticles with well-controlled size and shape are useful to understand the catalytic trends and design efficient catalysts [1,2]. However, nanoparticles have always been suspected whether their initial morphologies remain intact during the catalytic reactions. Small-sized particles may agglomerate into larger ones or high-index facets may transform into lower-index facets through a thermodynamically driven spontaneous process during thermal reactions [3]. This phenomenon leads to a decline in catalytic performance and may influent their recycling process. Therefore, increasing efforts have been made by loading metal nanoparticles on various supports [4]. The supporting matrices documented in the literature typically exhibit low surface areas and nanoparticles are often embedded within these supports. This arrangement can lead to limited accessibility of the catalysts to their targets. Thus, supporting materials with a highly porous structure can offer numerous accessible channels for diffusion and transport, maximizing the catalytic potential of metal nanoparticles [5,6].

Cuprous oxide (Cu_2O) is one of the most intensively examined metal oxide semiconductor materials and has been applied in many fields such as sensors, photocatalysis and antibacterials [7-10]. The Cu_2O nanoparticles act as a catalyst in many organic reactions such as C–C, C–N and C–S bond formation [11]. Cuprous oxide (Cu_2O) is also extensively used as catalysts for many organic reactions such as reduction, oxidation, azide/alkyne cycloaddition, cross coupling, Ullmann

reaction, gas-phase reactions, electrocatalysis, photocatalysis, coupling reactions, water-gas shift reactions, *etc*. [12-21].

Thus, the low cost, highly efficient and simple methods of synthesis of Cu_2O makes it a popular choice for catalyst in organic reactions. In most of the coupling reactions Pd used as catalyst but it is toxic in nature and highly expensive. Due to its non-toxic and low cost, Kar & Srivastava [22] used the Cu_2O catalysts in place of Pd catalyst for coupling reactions. Moreover, in catalysis, the noble metal catalysts (Au, Ag, *etc*.) have been widely used due to their high selectivity and catalytic efficiency but these metals are of highly expensive which hinders its practical applications [23]. With a growing focus on cost-effectiveness, efficiency and sustainability, there is an increasing interest in using non-noble metal materials as substitutes. Copper is substituted for noble metals but it is easily oxidizable by the atmospheric air and moisture. To prevent this oxidation different types of capping reagents have been used [24]. Metal nanoparticles with nanometer-scale dimensions are unstable and self-aggregation due to their high surface energy and large specific surface area. This tendency can lead to reduced catalytic efficiency and affect their recyclability [25]. As a result, significant efforts have been directed towards loading metal nanoparticles onto various supports.

The Cu_2O-based catalysts supported on different supports have significant effects on catalysis. Generally used supports are Al_2O_3, SiO_2, MgO, activated carbon, *etc*. The main role of the supports is dispersing and stabilizing active species [26]. The carbon matrix will act as a support for an active catalyst and as a catalyst itself [27]. Carbon materials are widely used in catalysis due to their high specific surface area and well-developed pore structure [28]. Active carbons are characterized by a surface area between 300 and 3200 m^2/g, with high capacity and versatility to adsorb certain compounds [29]. The combination of Cu_2O (cuprous oxide) nanoparticles with activated carbon (AC) has become a significant area of research due to the synergistic effects that enhance the activity of Cu_2O. The deposition of Cu_2O nanoparticles onto activated carbon allows for the utilization of extensive surface area, porosity, and adjustable surface chemistry of activated carbon, resulting in the superior catalytic performance and increased stability during reaction conditions. The high surface area of activated carbon facilitates the fine dispersion of Cu_2O nanoparticles, promoting the activity with increasing the number of active sites and improving the contact between the catalyst and reactants. Moreoer, porous structure of activated carbon provides easy access for reactants and products, enhancing the mass transport. In environmental applications, Cu_2O nanoparticles on activated carbon have demonstrated promising role in waste water treatment [30], air purification [31] and the removal of pollutants such as radioactive iodine [32], organic compounds [33] and toxic gases [34]. In present work, Cu_2O nanoparticles were dispersed on activated carbon and studied their activity for triazole synthesis using Click reaction. The Cu_2O nanoparticles supported on the activated carbon materials used for various reactions like methanol oxidative carbonylation [35], reduction of 4-nitrophenol to 4-aminophenol [36], propargylamine synthesis [37], selective hydroamination [38], photocatalytic activity [39], aluminium-air batteries [40]. Cu_2O nanoparticles supported on activated carbon materials are also used in the glucose sensing [41]. Here in this research, the catalytic activity of the Cu_2O nanoparticles supported on activated carbon material were explored in Click reaction. The density functional theory (DFT) serves as a highly effective approach for understanding the reaction mechanisms involved in catalysis. The synergistic effects arising due to the Cu_2O nanoparticles supported on the activated carbon material were examined using DFT simulations.

EXPERIMENTAL

Preparation of activated carbon: Palmyra palm fruit shells (10 g) were weighed and mixed with 30 g of K_2CO_3 in mortar to ensure a more homogeneous dispersion. Subsequently, the mixture was transferred to a stainless steel reactor. This mixture was carbonized in N_2 flow 140 mL/min at 750 ºC. After carbonization, the solution was allowed to cool down to room temperature, filtered and washed repeatedly with deionized water and anhydrous alcohol until it reached neutral pH. The solid product obtained was dried in a hot air oven at 80 ºC for 12 h. Subsequently, the solid was also washed with a 10% HCl to remove inorganic salts present in it. Again, it was washed with deionized water until the filtrate reached neutral pH. After drying in an oven at 80 ºC for 12 h, K_2CO_3 activated carbon obtained is indicated as PS-750-1-3. The different loadings of Cu_2O were deposited on carbon by wet impregnation method [42]. Highly stable nitrogen doped carbon encapsulated nano Cu_2O discs were synthesized and impregnated on the carbon support on different 5%, 10%, 15% concentrations and denoted as $5Cu_2O$-AC, $10Cu_2O$-AC and $15Cu_2O$-AC, respectively.

Characterization: As prepared activated carbon and Cu_2O supported on activated carbon (Cu_2O-AC) catalyst were characterized using the following instrumental techniques. Rigaku XRD 6000 diffractometer with Ni filtered Cu$K\alpha$ radiation at 40 kV, 30 mA was used for X-ray diffraction analysis. FT-IR spectrophotometer (IR prestige-21, Shimadzu, Japan) was used for the functional group analysis using KBr powder in the wavelength 4000-400 cm^{-1} range. The morphology of the activated carbon and XCu_2O-AC catalysts was characterized by a Zeiss EVO-50 Field Emission Scanning Electron Microscope (FESEM), model Supra 55 VP instrument. The Gaussian09 software [43] was used for all of the computational parameters described in this study. The computational approach was DFT/B3LYP/6-31 G (d,p), where DFT stands for density functional theory, B3 for Beck's three-parameter hybrid exchange functional [44], LYP for the Lee-Yang-Parr gradient-corrected correlation functional [45] and 6-31G(d,p) for the augmented split valence basis set used in the calculations. The initial structural characteristics for the target molecule were needed in order to start the geometry optimization process. Following standard procedures, Gauss View was used in absence of the experimental structural data [46].

Catalytic activity: The catalyst activity was investigated in batch reaction method. The catalyst (5 mg) was taken in a 50 mL round bottom flask containing 4-nitroazido benzene (5 mmol), prop-2-yn-1-ol (5 mmol) and 5 mL of solvent (DMF,

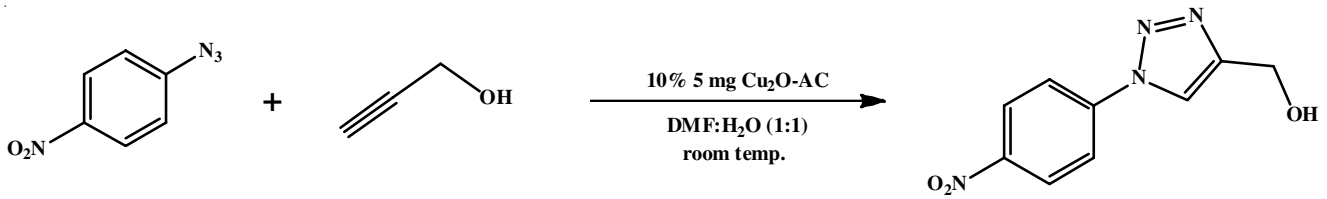

Scheme-I: Triazole synthesis using 10% Cu_2O-AC catalyst in 1:1 DMF-water solvent

EtOH and H_2O). The reaction was continued for 60 min with continuous stirring at room temperature. The progress of the reaction was monitored using TLC method (**Scheme-I**).

RESULTS AND DISCUSSION

X-ray diffraction studies: An X-ray diffraction analysis was performed on activated carbon and XCu_2O-AC (X = 5, 10, 15) within the 10º to 90º 2θ range to identify the phase of the support as well as copper oxide present on the activated carbon. Fig. 1a showed the amorphous nature of the support carbon. The activated carbon has two broad peaks in 2θ with peak maximum at 25º to 45º corresponds to the 002 and 101 planes respectively, it resembles the graphite hexagonal structure of the support carbon [47]. The XRD pattern of the Cu_2O-AC exhibits four diffraction peaks that can be indexed to Cu_2O at specific 2θ values at 36.60º (111), 42.40º (200), 61.50º (220), 73.69º (311), which indicates the presence of the Cu_2O phase with a cubic lattice structure [48]. As the weight percentage of Cu_2O increases the intensity of the cuprous oxide peaks increases from $5Cu_2O$-AC to $15Cu_2O$-AC. Broadness of the peaks indicates the material present in the XRD amorphous *i.e.* nanosized.

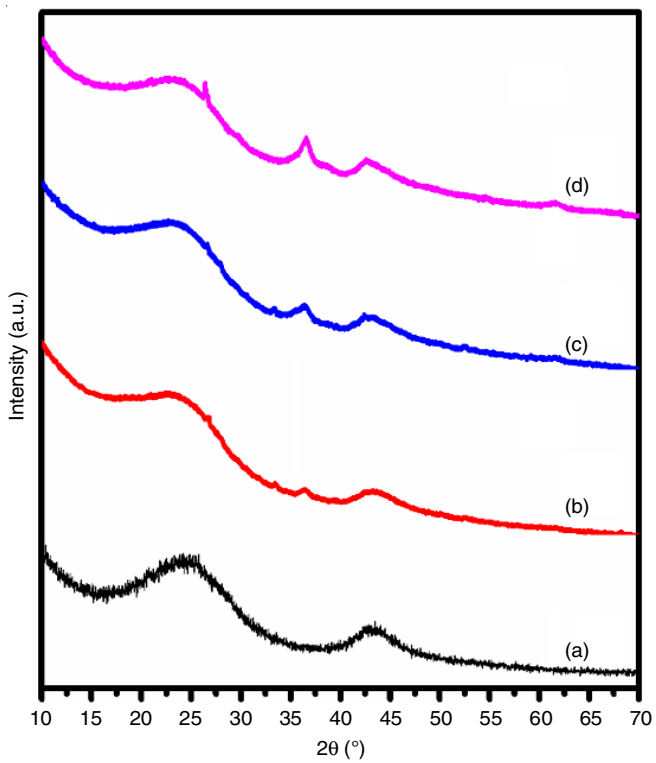

Fig. 1. X ray diffraction patterns of (a) activated carbon, (b) $5Cu_2O$-AC, (c) $10Cu_2O$-AC and (d) $15Cu_2O$-AC

FTIR studies: In the FTIR spectra within the 3750-3000 cm^{-1} range, a broad band corresponding to the hydroxyl (–OH) group is observed, indicating the presence of hydroxyl functionalities (Fig. 2). The peaks at 1604 cm^{-1} and 1409 cm^{-1} are attributed to C=C stretching vibrations and C–H bending modes, respectively, suggesting the presence of aromatic or unsaturated structures in the sample. Moreover, the region between 500-700 cm^{-1} is indicative of the C–O stretching vibrations, which further supports the presence of oxygenated functional groups [49]. Signficantly, the peak at 625 cm^{-1} is the characteristic of Cu_2O, confirming the presence of copper(I) oxide in the sample [50].

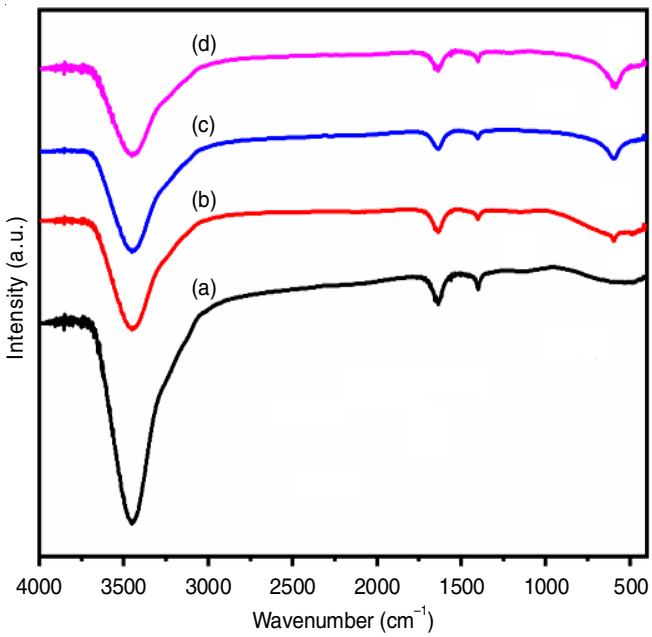

Fig. 2. FT-IR spectral patterns of (a) activated carbon, (b) $5Cu_2O$-AC, (c) $10Cu_2O$-AC and (d) $15Cu_2O$-AC

SEM studies: SEM images of the XCu_2O-AC (X = 5, 10, 15) sample are shown in Fig. 3. These micrographs reveal that the external surface of the activated carbons displays cracks, crevices and grains of varying sizes, along with porous structure. The SEM images were taken samples after carbonization at 750 ºC suggests that a porous structure was formed as most of the volatile compounds were escaped, leaving behind a ruptured activated carbon surface. The Cu_2O decorated activated carbon samples exhibit the spherical shape Cu_2O nanoparticles. At high concentration of Cu_2O loading shows the aggregation of nanoparticles. At 10 % concentration of Cu_2O loading nanoparticles are embedded uniformly in mesoporous activated carbon. Presence of nitrogen, carbon, oxygen and copper in

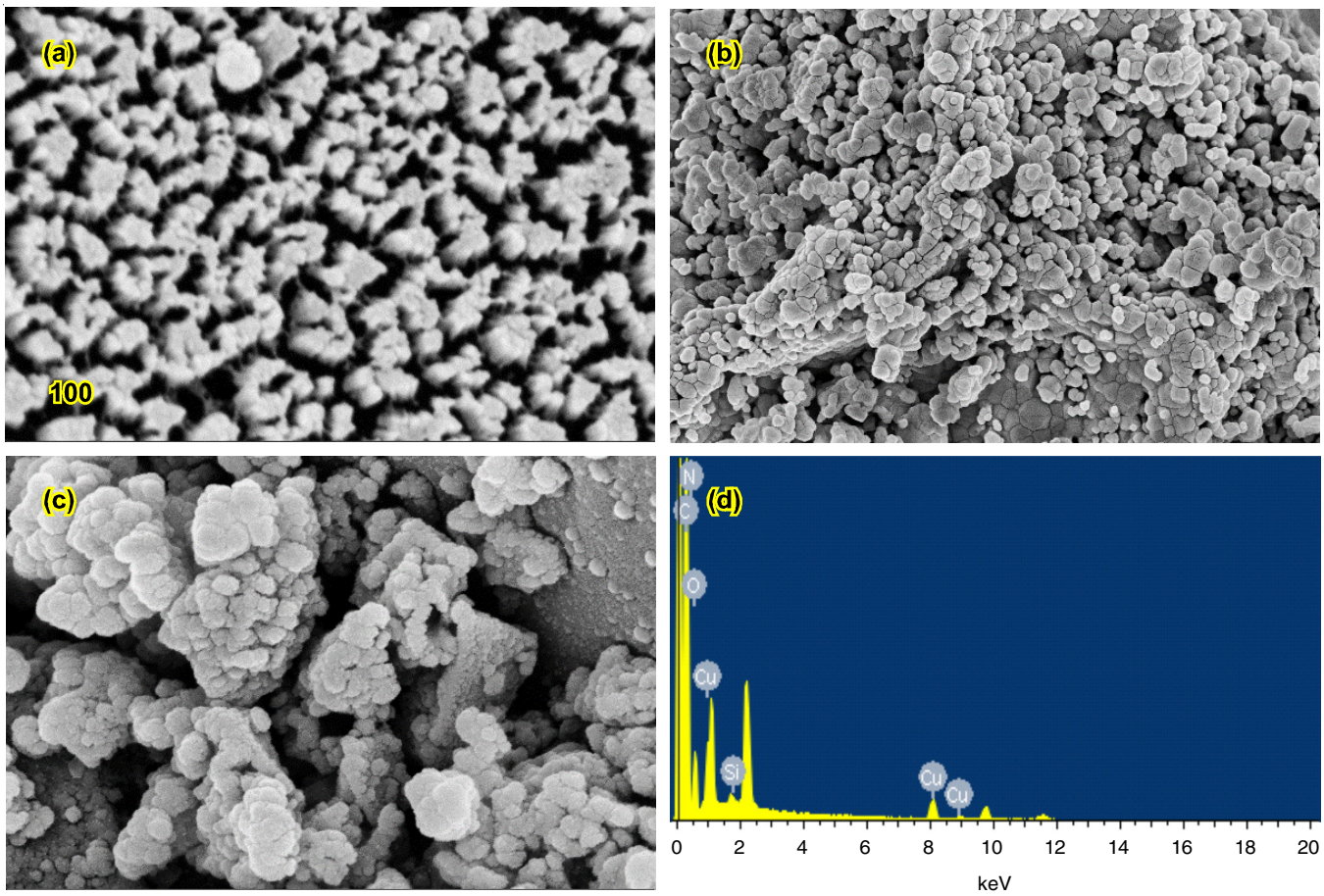

Fig. 3. SEM micrographs and EDX spectrum of 15Cu_2O-AC sample

the sample confirmed as observed from the SEM-EDX spectrum (Fig. 3d).

Click reaction-catalytic activity of Cu_2O-AC: Catalytic activities of Cu_2O-AC samples were studies in synthesis of triazoles. Initially, we carried out the reactions of 4-nitro azido benzene (5 mmol) and prop-2-yn-1-ol (5 mmol) with 5 mg of 5% Cu_2O-AC catalyst under DMF solvent at room temperature. Time taken for the reaction to complete is 80 min, 60% yield was obtained. Above same reaction was also carried out with 10% Cu_2O-AC, this reaction completed in 60 min with 88% yield. As percentage of Cu_2O increased on AC the reaction time is decreased and product yield increased. At 15% Cu_2O-AC reaction completed 60 min, 88% yield of product was isolated. It was observed that 10% Cu_2O-AC catalyst is enough for the triazole synthesis. Optimization of the Cu_2O loading was given in Fig. 4a. This reaction was carried out in different solvents EtOH and H_2O the product yield in EtOH obtained was 70% and in H_2O is 65%. DMF and H_2O 1:1 (v/v) ratio the product yield obtained was 90 %. The EtOH and H_2O the reaction yield is 85 %. The excellent yield obtained in the DMF and H_2O 1:1 (v/v) ratio. The same catalyst after completion of the reaction was filtered and reused. No significant change in the yield of the triazole was observed up to five cycles; however, after the fifth cycle, the percentage yield of the product decreased. For the reusability test, the catalyst demonstrated continuous activity for up to five cycles, as shown in Fig. 4b.

DFT studies: Fig. 5 shows the gas phase optimized structures of propargyl alcohol, nitro azidobenzene and the resultant product. Reactant and product bond lengths and angles alter as a result of product formation (Table-1). Among the three catalysts, only Cu_2O-AC nanocomposites showed the highest activity compared to activated carbon and/or Cu_2O nanoparticles. This enhancement in activity can be attributed to the strong π–π electron interaction between AC-Cu_2O nanocomposite, which supports with nitro azidobenzene organic molecules by which it can easily adsorb the substrate molecule.

The molecular electrostatic potential (MEP) maps of propargyl alcohol, *p*-nitro azidobenzene and the product ratio are illustrated in Fig. 6. Using molecular electrostatic potential, electron-rich or electron-deficient areas suitable for electrophilic or nucleophilic assault may be identified by the circulation of positive and negative potential across a system [51]. The MEP surfaces are labelled with a variety of colours; the neutral zone is shown by green, while the most positive and negative sections are shown by blue and red. Propargyl alcohol may function as a nucleophile if it exhibits a red coloration on the alkyne group. The blue colour of the benzene moiety group in *p*-niro azidobenzene indicates that it is the electrophile.

A substantial amount of the contributions to molecular interactions with other species are attributed to frontier molecular orbitals [52]. Electron donation is represented by the highest occupied molecular orbital (HOMO), whereas electron

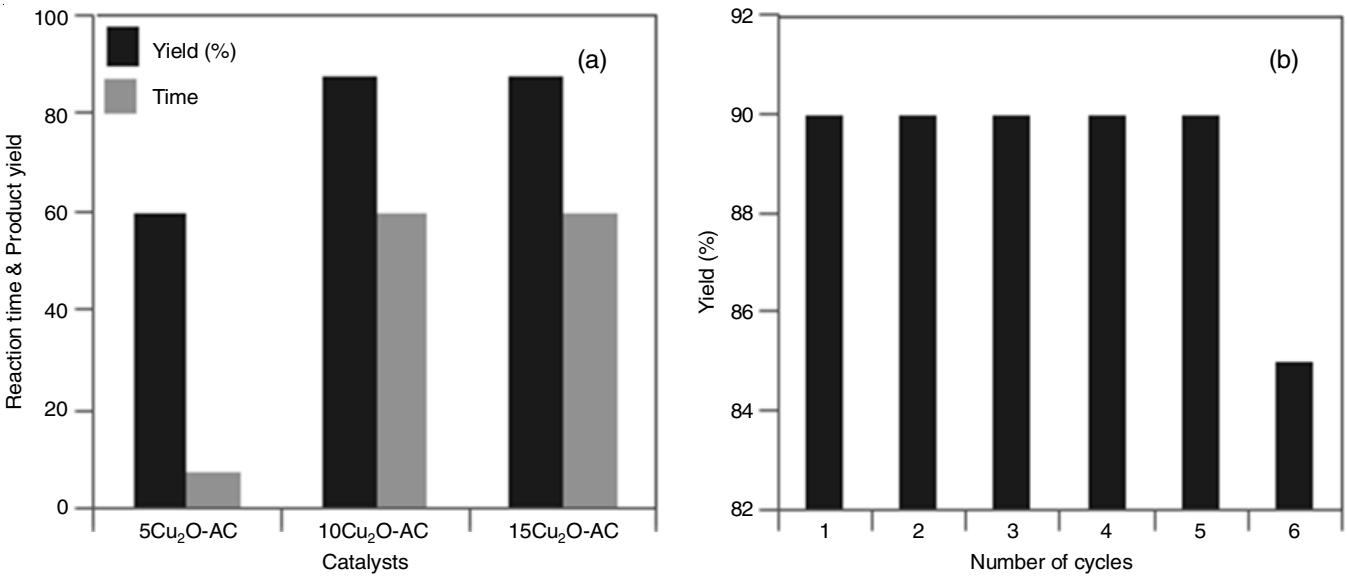

Fig. 4. (a) Optimization of the Cu_2O loading and (b) reusability of the catalyst $10Cu_2O$-AC

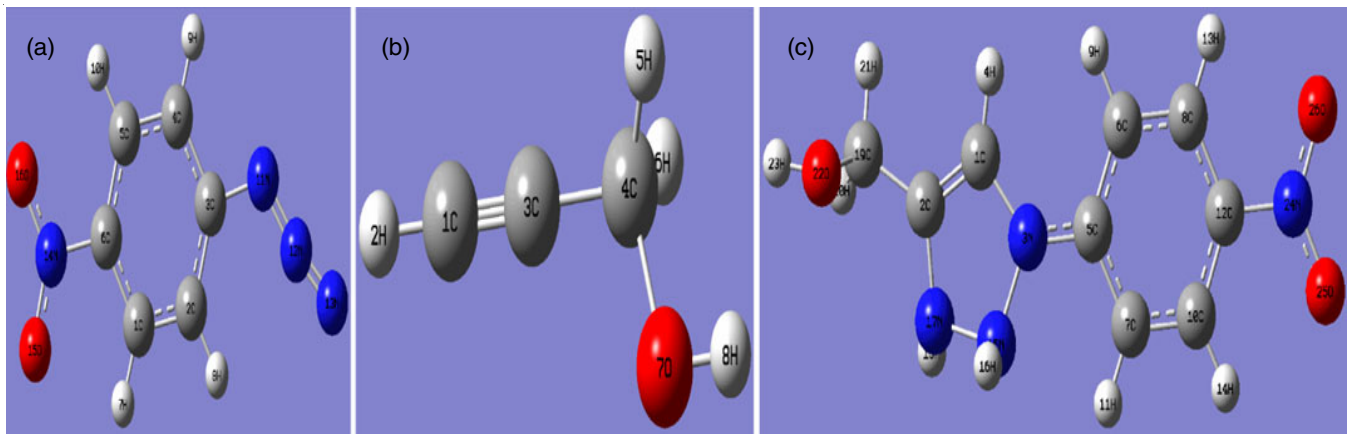

Fig. 5. Optimized structures of (a) *para*-nitro azido benzene, (b) propargyl alcohol and (c) resultant product

TABLE-1
OPTIMIZED STRUCTURAL PARAMETERS OF MOLECULE–BOND LENGTH (Å) AND BOND ANGLE (°) AS PREDICTED BY DFT/B3LYP/6-31 G(d,p)

Bond	Bond length (Å)	Bond	Bond length (Å)	Bond	Bond length (Å)	Bond	Bond length (Å)
C1-C2	1.382	N7-C8	1.382	C12-O13	1.472	C8-H19	1.022
C2-C3	1.384	C8-C9	1.354	C1-H14	1.034	N10-H20	1.022
C3-C4	1.389	C9-N10	1.432	C2-H15	1.056	N11-H21	1.033
C4-C5	1.402	N10-N11	1.469	C3-H16	1.098	C12-H22	1.045
C5-C6	1.411	N11-N7	1.477	C4-H17	1.074	C12-H23	1.076
C6-C1	1.399	C9-C12	1.427	C6-H18	1.063	O13-H24	0.753
C5-N7	1.372	–	–	–	–	–	–
Bond	Bond angles (°)	Bond	Bond angles (°)	Bond	Bond angles (°)	Bond	Bond angles (°)
C1-C2-C3	120.6	C1-C6-H18		C2-C3-H16	123.1	N11-N10-C9	120.6
C2-C3-C4	116.9	C5-C6-H18	122.1	C3-C2-H15	122.9	N10-C9-C8	116.9
C3-C4-C5	119.9	C6-C5-N7	116.9	C1-C2-H15	122.9	C9-C8-C7	119.9
C4-C5-C6	123.4	C4-C5-N7	122.1	C2-C1-H14	115.8	C5-N7-N11	123.4
C5-C6-C1	123.6	C5-C4-H17	122.1	C6-C1-H14	115.8	C5-N7-C8	123.6
C6-C1-C2	119.8	C3-C4-H17	121.8	C8-N7-N11	123.7	N10-N11-H21	119.8
C2-C1-H14	120.8	C4-C3-H16	123.2	N7-N11-N10	122.3	N7-N11-H21	120.8
C6-C1-H14	120.3	–	–	–	–	–	–

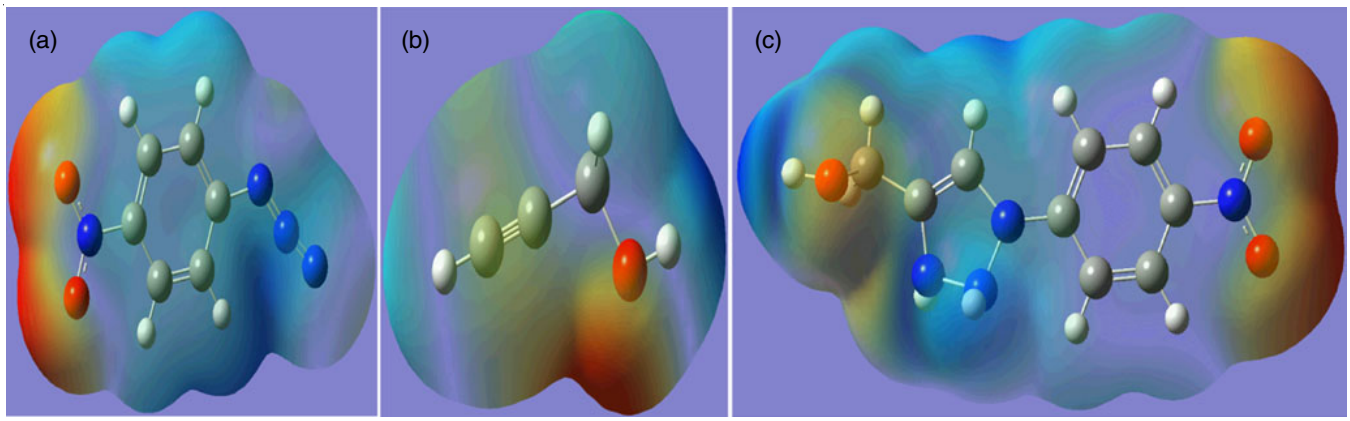

Fig. 6. Molecular electrostatic potential maps of (a) *para*-nitro azido benzene, (b) propargyl alcohol and (c) resultant product

uptake is represented by the lowest unoccupied molecular orbital (LUMO), which are shown in Fig. 7. While the LUMO was mostly found on the benzene molecule, the product HOMO was mostly found around the triazole ring.

Fig. 8 shows the Mulliken effective charge for the product, as well as azidobenzene and propargyl alcohol in the gas phase. These Mulliken atomic charges were found using DFT. The main differences can be seen both before and after the reactive molecules have been complexed.

Conclusion

In present work, an economic, practically viable Cu_2O nanoparticles supported on mesoporous activated carbon as catalysts were prepared successfully for the synthesis of triazoles using

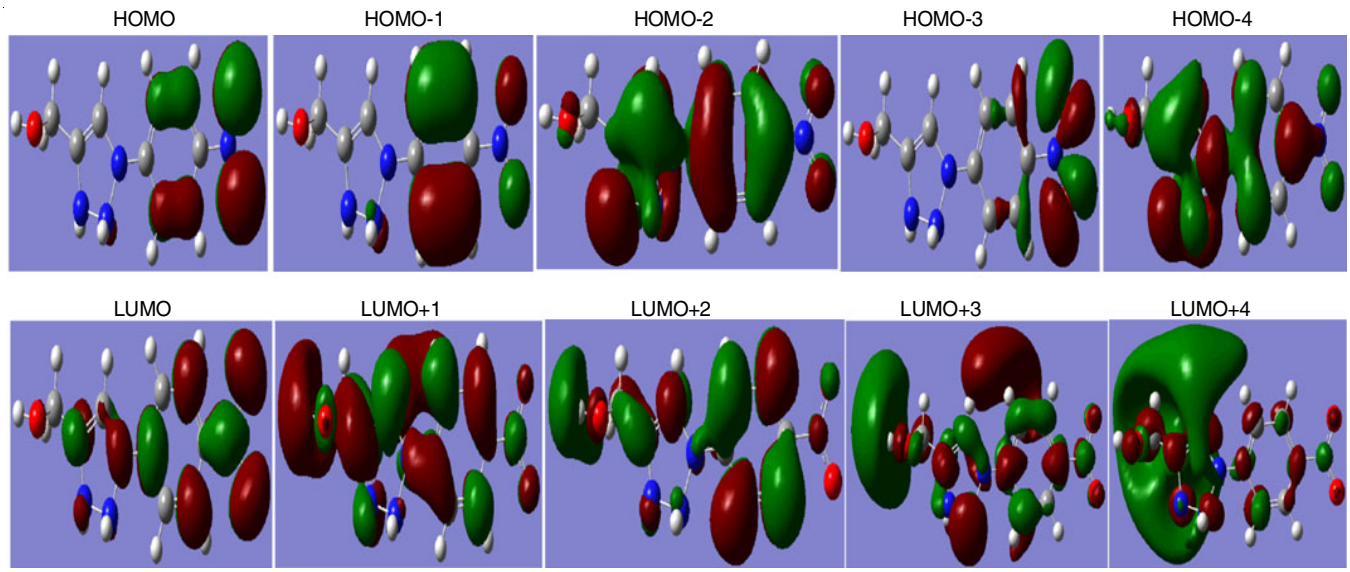

Fig. 7. Frontier molecular orbital pictures of resulting product

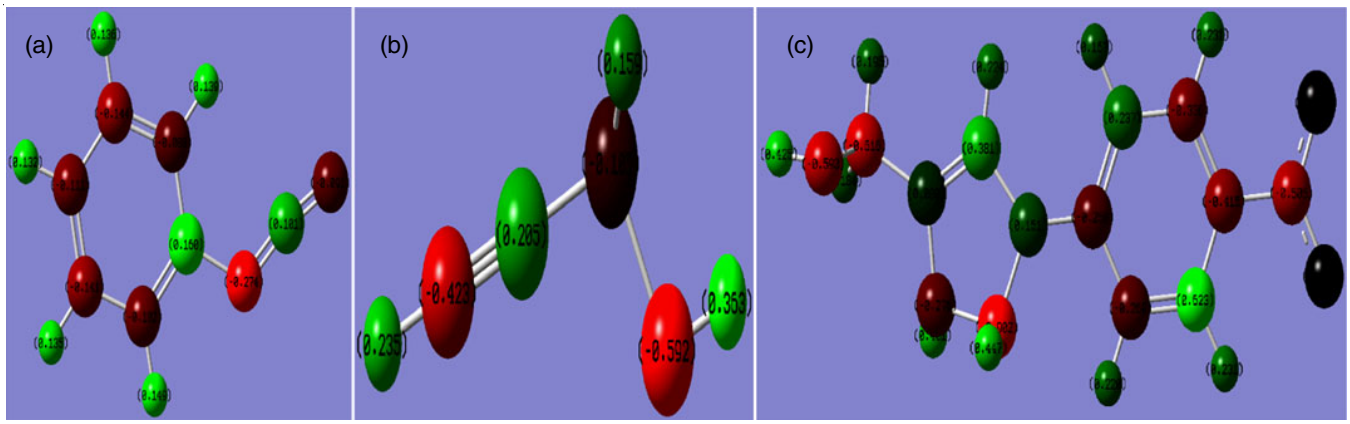

Fig. 8. Mulliken atomic charges of (a) azido benzene, (b) propargyl alcohol and (c) resultant product

Click reaction. Activated carbon derived from the shell of palmyra palm fruit has served as a support for the dispersion of cuprous oxide nanoparticles. The XRD and FT-IR analyses characterized the Cu_2O-AC nanocomposites. Topographic, morphological information of the carbon was observed from the SEM images. Good yield of triazole was achieved with 10% Cu_2O on active carbon sample. DFT analysis shows that the synergistic effect between the surface of Cu_2O-AC, propargyl alcohol and *p*-nitro azidobenzene to form triazoles.

CONFLICT OF INTEREST

The authors declare that there is no conflict of interests regarding the publication of this article.

REFERENCES

1. Y. Zhou, C. Jin, Y. Li and W. Shen, *Nanotoday*, **20**, 101 (2018); https://doi.org/10.1016/j.nantod.2018.04.005
2. B.R. Cuenya and F. Behafarid, *Surf. Sci. Rep*., **70**, 135 (2015); https://doi.org/10.1016/j.surfrep.2015.01.001
3. H. Jung, S.Y. Lee, C.W. Lee, M.K. Cho, D.H. Won, C. Kim, H.-S. Oh, B.K. Min and Y.J. Hwang, *J. Am. Chem. Soc.*, **141**, 4624 (2019); https://doi.org/10.1021/jacs.8b11237
4. H. Hu, S. Lu, T. Li, Y. Zhang, C. Guo, H. Zhu, Y. Jin, M. Du and W. Zhang, *Nanoscale Adv.*, **3**, 1865 (2021); https://doi.org/10.1039/D1NA00025J
5. M. Sankar, Q. He, R.V. Engel, M.A. Sainna, A.J. Logsdail, A. Roldan, D.J. Willock, N. Agarwal, C.J. Kiely and G.J. Hutchings, *Chem. Rev.*, **120**, 3890 (2020); https://doi.org/10.1021/acs.chemrev.9b00662
6. P. Bernard, P. Stelmachowski, P. Bros, W. Makowski and A. Kotarba, *J. Chem. Educ.*, **98**, 935 (2021); https://doi.org/10.1021/acs.jchemed.0c01101
7. J. Choi, N. King and P.A. Maggard, *ACS Nano*, **7**, 1699 (2013); https://doi.org/10.1021/nn305707f
8. S. Deng, V. Tjoa, H.M. Fan, H.R. Tan, D.C. Sayle, M. Olivo, S. Mhaisalkar, J. Wei and C.H. Sow, *J. Am. Chem. Soc.*, **134**, 4905 (2012); https://doi.org/10.1021/ja211683m
9. M.R. Dustgeer, S.T. Asma, A. Jilani, K. Raza, S.Z. Hussain, M.B. Shakoor, J. Iqbal, M.S. Abdel-Wahab and R. Darwesh, *Inorg. Chem. Commun.*, **128**, 108606 (2021); https://doi.org/10.1016/j.inoche.2021.108606
10. K. Wang, M. Lv, T. Si, X. Tang, H. Wang, Y. Chen and T. Zhou, *J. Hazard. Mater.*, **461**, 132479 (2024); https://doi.org/10.1016/j.jhazmat.2023.132479
11. A.Y. Mitrofanov, A.V. Murashkina, I. Martín-García, F. Alonso and I.P. Beletskaya, *Catal. Sci. Technol.*, **7**, 440 (2017); https://doi.org/10.1039/C7CY01343D
12. S. Ferdousi, M.S. Alam, E. Ahmmed, R.S. Brishti and M.A.R. Khan, *Results in Chemistry*,**13**,101935 (2024); https://doi.org/10.1016/j.rechem.2024.101935
13. M.J. Bröcker, J.M.L. Ho, G.M. Church, D. Söll and P. O'Donoghue, *Angew. Chem.*, **126**, 1 (2014); https://doi.org/10.1002/ange.201310509
14. S. Ghosh, S. Saha, D. Sengupta, S. Chattopadhyay, G. De and B. Basu, *Ind. Eng. Chem. Res.*, **56**, 11726 (2017); https://doi.org/10.1021/acs.iecr.7b02656
15. D. Chakraborty, S. Nandi, D. Mullangi, S. Haldar, C.P. Vinod and R. Vaidhyanathan, *ACS Appl. Mater. Interfaces*, **11**, 15670 (2019); https://doi.org/10.1021/acsami.9b02860
16. M. Li, X. Xing, Z. Ma, J. Lv, P. Fu and Z. Li, *ACS Sustain. Chem.& Eng.*, **6**, 5495 (2018); https://doi.org/10.1021/acssuschemeng.8b00350
17. Lili Wan1, QixingZhou, Xin Wang, Thomas E. Wood, Lu Wang, Paul N,http://www.nature.com/natcatal, https://doi.org/10.1038/s41929-019-0338-z
18. Safieh Momeni, Fatemeh Sedaghati, Microc (2018); https://doi.org/10.1016/j.microc.2018.07.035
19. A. Kerour, S. Boudjadar, R. Bourzami and B. Allouche, *J. Solid State Chem.*, **263**, 79 (2018); https://doi.org/10.1016/j.jssc.2018.04.010
20. R.T. Addanki Tirumala, A. P. Dadgar, F. Mohammadparast, T. Mou, S.B. Ramakrishnan, B. Wang and M. Andiappan, *Green Chem.*, **21**, 5284 (2019); https://doi.org/10.1039/C9GC01930H
21. S.D. Senanayake, D. Stacchiola and J.A. Rodriguez, *Acc. Chem. Res.*, **46**, 1702 (2013); https://doi.org/10.1021/ar300231p
22. A.K. Kar and R. Srivastava, *Inorg. Chem. Front.*, **6**, 576 (2019); https://doi.org/10.1039/C8QI01198B
23. C.W. Thurner, N. Bonmassar, D. Winkler, L. Haug, K. Ploner, P.D.K. Nezhad, X. Drexler, A. Mohammadi, P.A. van Aken, J. Kunze-Liebhäuser, A. Niaei, J. Bernardi, B. Klötzer and S. Penner, *ACS Catal.*, **12**, 7696 (2022); https://doi.org/10.1021/acscatal.2c01584
24. R. Javed, M. Zia, S. Naz, S.O. Aisida, N. Ain and Q. Ao, *J. Nanobiotechnology*, **18**, 172 (2020); https://doi.org/10.1186/s12951-020-00704-4
25. Q-L. Zhu and Q. Xu, *Chem*, **1**, 220 (2016); https://doi.org/10.1016/j.chempr.2016.07.005
26. S. Biswas, A. Pal and T. Pal, *RSC Adv.*, **10**, 35449 (2020); https://doi.org/10.1039/D0RA06168A
27. M.J. Illán-Gómez, S. Brandán, C. Salinas-Martínez de Lecea and A. Linares-Solano, *Fuel*, **80**, 2001 (2001); https://doi.org/10.1016/S0016-2361(01)00091-6
28. M.J. Illan-Gomez, A. Linares-Solano, C.S.-M. de Lecea and J.M. Calo, *Energy Fuels*, **7**, 146 (1993); https://doi.org/10.1021/ef00037a023
29. G. Li, A. Iakunkov, N. Boulanger, O.A. Lazar, M. Enachescu, A. Grimm and A.V. Talyzin, *RSC Adv.*, **13**, 14543 (2023); https://doi.org/10.1039/D3RA00820G
30. G. Tiwari, R.R. Devi, S.P. Mahanta, P.K. Raul, S. Chatterjee and D.V. Kamboj, *Inorg. Chem. Commun.*, **152**, 110687 (2023); https://doi.org/10.1016/j.inoche.2023.110687
31. C. Boruban and E.N. Esenturk, *J. Nanopart. Res.*, **20**, 59 (2018); https://doi.org/10.1007/s11051-018-4139-0
32. X. Zhang, P. Gu, X. Li and G. Zhang *Chem. Eng. J.*, **322**, 129 (2017); https://doi.org/10.1016/j.cej.2017.03.102
33. J. Li, L. Huang, X. Jiang, L. Zhang and X. Sun, *Chem. Eng. J.*, **404**, 127091 (2021); https://doi.org/10.1016/j.cej.2020.127091
34. M. Saad, A. Szymaszek, A. Bialas, B. Samojeden and M. Motak, *Catalysts*, **10**, 1426 (2020); https://doi.org/10.3390/catal10121426
35. J. Wang, T. Fu, F. Meng, D. Zhao, S.S.C. Chuang and Z. Li, *Appl. Catal. B*, **303**, 120890 (2022); https://doi.org/10.1016/j.apcatb.2021.120890
36. H. Niu, S. Liu, Y. Cai, F. Wu and X. Zhao, *Micropor. Mesopor. Mater.*, **219**, 48 (2016); https://doi.org/10.1016/j.micromeso.2015.07.027
37. A.V. Nakhate and G.D. Yadav, *Mol. Catal.*, **451**, 209 (2018); https://doi.org/10.1016/j.mcat.2018.01.013
38. S.-L. Shi and S.L. Buchwald, *Nat. Chem.*, **7**, 38 (2015); https://doi.org/10.1038/nchem.2131
39. Y. Liu, Q. Huang, G. Jiang, D. Liu and W. Yu, *J. Mater. Res.*, **32**, 3605 (2017); https://doi.org/10.1557/jmr.2017.307
40. J. Tian, D. Liu, J. Li, D. Sun, H. Liu, H. Wang and Y. Tang, *Chin. Chem. Lett.*, **32**, 2427 (2021); https://doi.org/10.1016/j.cclet.2021.01.022
41. M. Waqas, L. Wu, H. Tang, C. Liu, Y. Fan, Z. Jiang, X. Wang, J. Zhong and W. Chen, *ACS Appl. Nano Mater.*, **3**, 4788 (2020); https://doi.org/10.1021/acsanm.0c00847
42. R. Anumandla, P. Shanigaram, R. Samineni and S. Veldurthi, A Method to Prepare Highly Stable Carbon Encapsulated Nano Cu_2O Spheres (CEN-Cu_2O spheres), Indian Patent no. 551165 (2024).

43. M.J. Frisch, G.W. Trucks, H.B. Schlegel, G.E. Scuseria, M.A. Robb, J.R. Cheeseman, G. Scalmani, V. Barone, B. Mennucci, G.A. Petersson, H. Nakatsuji, M. Caricato, X. Li, H.P. Hratchian, A.F. Izmaylov, J. Bloino, G. Zheng, J. L. Sonnenberg, M. Hada, M. Ehara, K. Toyota, R. Fukuda, J. Hasegawa, M. Ishida, T. Nakajima, Y. Honda, O. Kitao, H. Nakai, T. Vreven, J.A. Montgomery, Jr., J.E. Peralta, F. Ogliaro, M. Bearpark, J.J. Heyd, E. Brothers, K.N. Kudin, V.N. Staroverov, T. Keith, R. Kobayashi, J. Normand, K. Raghavachari, A. Rendell, J.C. Burant, S.S. Iyengar, J. Tomasi, M. Cossi, N. Rega, J.M. Millam, M. Klene, J.E. Knox, J.B. Cross, V. Bakken, C. Adamo, J. Jaramillo, R. Gomperts, R.E. Stratmann, O. Yazyev, A.J. Austin, R. Cammi, C. Pomelli, J.W. Ochterski, R.L. Martin, K. Morokuma, V.G. Zakrzewski, G.A. Voth, P. Salvador, J.J. Dannenberg, S. Dapprich, A.D. Daniels, O. Farkas, J.B. Foresman, J. V. Ortiz, J. Cioslowski and D.J. Fox, Gaussian 09, Revision B.01, Gaussian, Inc., Wallingford CT (2010).
44. A.D. Becke, *J. Chem. Phys.*, **98**, 5648 (1993); https://doi.org/10.1063/1.464913
45. C. Lee, W. Yang and R.G. Parr, *Phys. Rev. B Condens. Matter*, **37**, 785 (1988); https://doi.org/10.1103/PhysRevB.37.785
46. R. Dennington, T. Keith and J. Millam, Gauss View, Version 5.0, Semichem Inc, Shawnee Mission (2009).
47. S. Sonal, P. Prakash, B.K. Mishra and G.C. Nayak, *RSC Adv.*, **10**, 13783 (2020); https://doi.org/10.1039/C9RA10103A
48. B. Yan, S. Huang, S. Wang and X. Ma., *ChemCatChem*, **6**, 2671 (2014); https://doi.org/10.1002/cctc.201402201
49. Z. Lendzion-Bieluñ, L. Czekajlo, D. Sibera, D. Moszyñski, J. Sreñscek-Nazzal, A.W. Morawski, R.J. Wrobel, B. Michalkiewicz, W. Arabczyk and U. Narkiewicz, *Adsorpt. Sci. Technol.*, **36**, 478 (2018); https://doi.org/10.1177/0263617417704527
50. R. Anumandla, P. Shanigaram, R. Samineni, M. Varukolu, S.K. D, P. Kokku, S. Challapalli and S. Veldurthi, *J. Mol. Struct.*, **1321**, 139798 (2025); https://doi.org/10.1016/j.molstruc.2024.139798
51. M. Varukolu, M. Palnati, V. Nampally, S. Gangadhari, M. Vadluri and P. Tigulla, *ACS Omega*, **7**, 810 (2022); https://doi.org/10.1021/acsomega.1c05464
52. V. Mahipal, N. Venkatesh, B. Naveen, G. Suresh, V. Manaiah and T. Parthasarathy, *Chem. Data.Coll.*, **28**, 100474 (2020); https://doi.org/10.1016/j.cdc.2020.100474